

# Investigation of contact deformation and wear characteristics of discrete track recording media

Y. Yoon · F. E. Talke

Received: 7 July 2010 / Accepted: 21 January 2011 / Published online: 11 February 2011  
© The Author(s) 2011. This article is published with open access at Springerlink.com

**Abstract** The contact deformation and wear characteristics of smooth and discrete track recording (DTR) media are investigated using nano-indentation and nano-scratch testing. Plastic deformation of the land areas between adjacent grooves was found to be substantially larger than in the smooth regions of the same disk. Reciprocating wear tests showed that wear was more severe for discrete track disks than for smooth disks. To improve the tribology of DTR media, planarization of discrete track disks appears to be necessary.

## 1 Introduction

Discrete track recording (DTR) technology has recently received renewed interest as a promising approach to increase the areal density in hard disk drives (Weller and Moser 1999; Greaves and Muraoka 2006). In DTR, adjacent tracks are separated from each other by circular “grooves” causing a reduction in “cross-talk” and an improvement in the signal to noise ratio (SNR) (Wachenschwanz et al. 2005). DTR technology has the potential of achieving areal densities in excess of 1 Tbit/in<sup>2</sup>. One of the key requirements for achieving areal densities in excess of 1 Tbit/in<sup>2</sup> is that the separation between the recording slider and the disk should be on the order of 1 nm (Juang et al. 2007). The reduction of

flying height from presently 5 nm to the 1 nm regime increases the likelihood of intermittent contacts, loss of data and failure of a hard disk drive. To prevent failure, improvements in the wear characteristics of the head disk interface are essential. Many researchers have studied the effect of slider/disk contacts (Komvopoulos 2000; Wang et al. 2001; Kohira et al. 2001; Xu et al. 2002) for conventional “smooth” media. However, little information is available on the problem of slider/disk contacts in the case of DTR media. Gong and Komvopoulos investigated numerically the contact deformation of patterned media (Gong and Komvopoulos 2003). Using finite element analysis, they observed that high pressure peaks at the edges of the bit pattern are present. Nunez et al. (2008) simulated numerically the contact behavior of patterned media after planarization. They found that planarization improves the contact resistance compared to non-planarized patterned media since the planarization material participates in supporting the applied load during contact and reduces the contact stress of the patterned surface.

In this paper, the contact deformation and wear characteristics of smooth and DTR media are investigated using nano-indentation and nano-scratch testing (Jiang et al. 1995; Anokin et al. 1998; Li and Bhushan 1999; Sundararajan and Bhushan 1999; Bai et al. 2000; Bhushan 1999; Huang et al. 2001). The deformation of the land area between adjacent grooves is investigated as a function of land width and applied load. Comparison of the results with smooth media is performed. The dependence of wear characteristics on track geometry is investigated. Atomic force microscopy (AFM), in situ scanning probe microscopy (SPM) (Bhushan 2001) and scanning electron microscopy (SEM) are used to investigate wear and damage of individual discrete tracks.

Y. Yoon (✉) · F. E. Talke  
Center for Magnetic Recording Research,  
U. C. San Diego, La Jolla, CA 92093-0401, USA  
e-mail: paul@talkelab.ucsd.edu

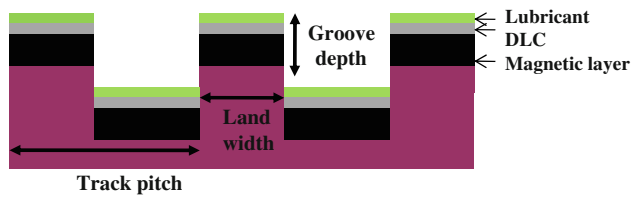


**Fig. 1** Typical discrete track recording disk

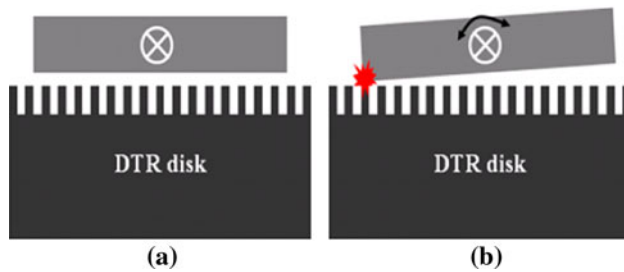


**Fig. 2** Schematic of head-disk interface for DTR disk: **a** stable flying and **b** contact with DTR disk

## 2 Experimental procedure

DTR disks were fabricated by nano-imprint lithography (NIP) (Wachenschwanz et al. 2005). The magnetic layer (20 nm), the diamond like carbon (DLC) layer (2 nm), and the lubricant film (1.2 nm) were deposited after nano-imprinting. The schematic of a typical DTR disk is shown in Fig. 1. DTR disks are characterized by land width, groove depth and track pitch.

### 2.1 Contacts between slider and DTR disk

In DTR, a slider flies over thousands of parallel discrete tracks during reading and writing.

Figure 2a shows the schematic of a slider flying over a DTR disk without contacts while Fig. 2b shows the situation when contacts between the slider and the DTR disk occur. Contacts between slider and disk cause wear of both the slider and the disk and increase the likelihood of failure of a hard disk drive. Therefore, the understanding of the contact behavior and wear characteristics of discrete track media is of great importance.

### 2.2 Nano-indentation and nano-scratch testing

To evaluate the tribology of discrete track media, nano-indentation and nano-scratch tests were performed as shown in Fig. 3a, b). In addition, load displacement curves (Fig. 3c) were obtained and analyzed in terms of maximum dissipated energy and residual deformation.

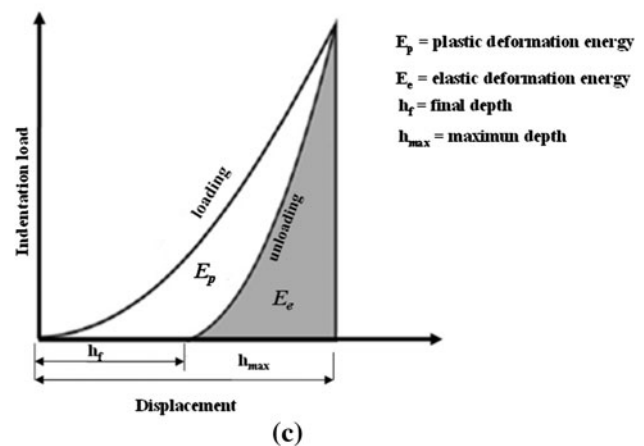
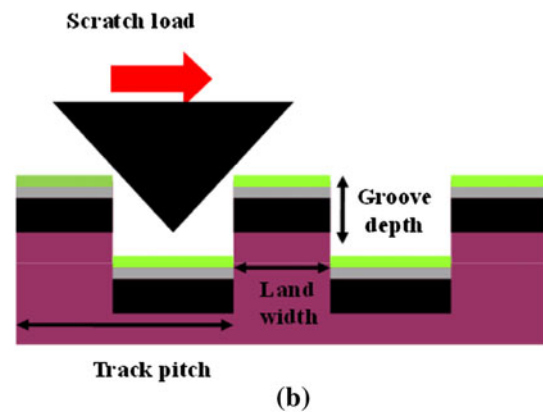
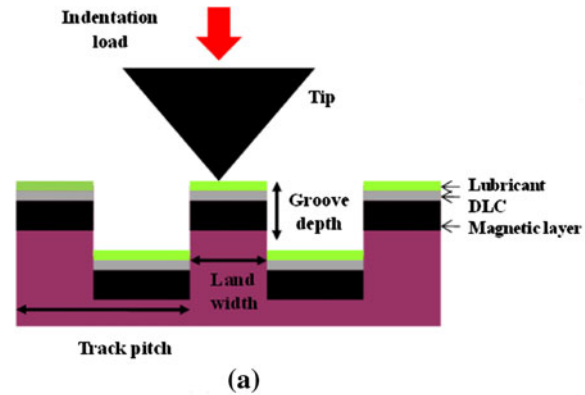


**Fig. 3** Schematic of nano-indentation and nano-scratch testing on discrete track disk: **a** schematic of nano-indentation, **b** schematic of nano-scratch testing and **c** typical load–displacement curve

### 2.3 Reciprocating wear testing

Reciprocating wear testing was used to evaluate the wear behavior of DTR disks. Figure 4 shows the schematic of the experimental setup (Huang et al. 2001). To create a reciprocating motion, a shear mode piezoelectric (PZT) actuator connected to a signal generator was used. The shear mode actuator was driven by a triangular input voltage signal from a signal generator (Fig. 4b). The

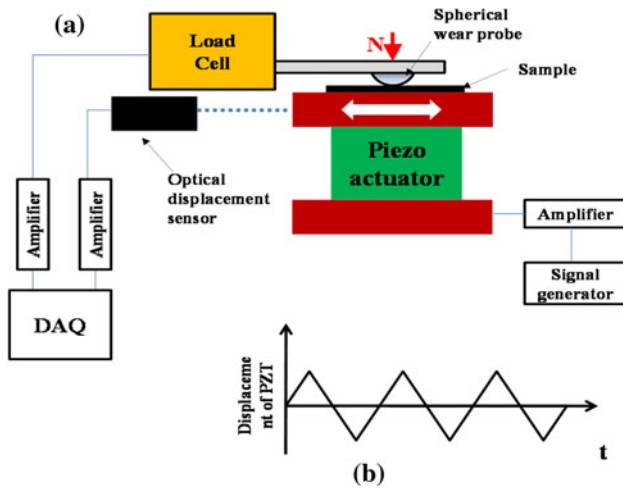


**Fig. 4** a Experimental setup and b displacement of PZT versus time

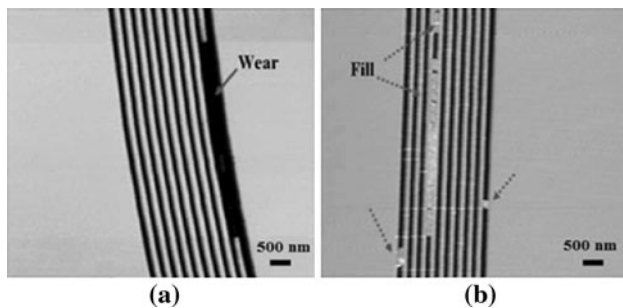


**Fig. 5** AFM images of worn tracks and accumulation of wear particles in discrete tracks: a wear of discrete tracks and b accumulation of wear particles in the grooves of discrete track media

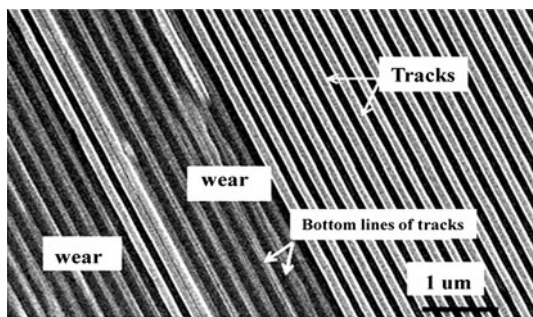


**Fig. 6** SEM image of worn DTR disk (groove depth = 40 nm, land width = 90 nm, track pitch = 200 nm)

displacement of the PZT actuator was measured using an optical displacement sensor (Fig. 4a). Disk samples (discrete track disk surfaces or smooth disk surfaces) were positioned on the top of the shear mode PZT as indicated in Fig. 4a. A normal force  $N$  was applied to the wear probe and a load cell was used to measure the friction as a function of the normal force and the number of wear cycles.

### 3 Experimental investigation

#### 3.1 Wear of DTR media due to contacts between slider and disk

A “sparsely” populated discrete track disk (Fig. 5), with a limited number of tracks (land width = 198 nm, groove depth = 63 nm and track pitch = 380 nm), was used in this part of the investigation. Initially, the disk was accelerated to a velocity of 24 m/s and a typical pico slider was flown at zero skew angle on the disk. Then, the rotational speed of the disk was decreased until continuous contact between slider and disk was observed. In our experiments, continuous contact was found to occur at a velocity of 3.3 m/s (touch-down velocity).

Figure 5 shows AFM images of a worn discrete track disk. We observe that the discrete track region of the disk shows large scale wear and material removal as a result of continuous sliding between slider and disk (Fig. 5a). In addition, wear particles originating from damaged tracks were found to accumulate in the grooves of the discrete tracks (Fig. 5b). Similar wear results from flyability studies at 24 m/s are shown in Fig. 6, indicating that large regions of the discrete tracks have been removed.

If similar touch-down experiments were repeated on the same disk in the area outside of the discrete track region, no damage or wear was observed. Since the material properties of the disk are the same in the DTR area and the “smooth” area, it is apparent that the presence of grooves affects the contact and wear characteristics of DTR disks.

#### 3.2 Contact deformation of smooth and discrete track surfaces using nano-indentation and nano-scratch testing

In the next set of experiments, the contact characteristics of the land area of discrete tracks was investigated using a commercially available nano-indenter (Hysitron Inc., USA) with a cube corner diamond tip (radius = 60 nm). After each test, the experiments were repeated in the smooth area of the same disk, i.e., outside the discrete track region. To study the effect of geometry of discrete tracks, two different types of discrete track disks were used (Table 1). All discrete track disk samples were fabricated using the same manufacturing process. Nano-indentations were made in the center of the land of discrete tracks and nano-scratches were made in the direction perpendicular to the discrete tracks.

Figure 7a shows the micrograph of a typical indentation in the land area of a discrete track disk while Fig. 7b shows the micrograph of a scratch in the direction perpendicular to the discrete tracks. We observe from Fig. 7a that large scale plastic deformation is present. A similar conclusion

**Table 1** Characteristics of two different types of discrete track disk surfaces

	Discrete track A	Discrete track B
Land width (W)	198 nm	144 nm
Groove depth (D)	33 nm	63 nm
Track pitch (T)	380 nm	380 nm
Ratio (D/W) (groove depth/land width)	0.1667	0.4375

with respect to plastic deformation can also be made for the scratch shown in Fig. 7b. Figure 7c shows the cross section of the plastic deformation in the land area of the discrete track disk along the line ( $t_1 - t_2$ ) of Fig. 7a.

Figure 8 shows SPM images of nano-indentations for the smooth and the land area of a DTR disk. The images in the top row of Fig. 8 were obtained for loads ranging from 200 to 700  $\mu\text{N}$  in the smooth region of the disk. The images in the bottom row show the indentations in the narrow land area. We observe that the indentations in the smooth and the land area increase with load. Furthermore, we observe that the size of the deformation in the narrow land area is larger than the deformation in the smooth disk area, i.e., a large difference exists in the deformation characteristics of smooth and discrete track disks. Clearly, the indentation characteristics in the narrow track areas are affected by the geometry and the aspect ratio of the individual discrete tracks.

Figure 9 shows load–displacement curves for nano-indentations in the smooth area of DTR disk A. Figures 10 and 11 show similar curves taken in the land areas of DTR disks A and B, respectively, at loads ranging from 200 to 700  $\mu\text{N}$ . In the case of the smooth disk shown in Fig. 9, plastic behavior is small at a load of 200  $\mu\text{N}$ . A much larger plastic deformation is observed, however, at the same load of 200  $\mu\text{N}$  in the land area of DTR disks A and B (Figs. 10, 11). Furthermore, plastic deformation was found to increase with normal load in the land area of DTR disks A and B (Figs. 10, 11) in comparison to smooth disks. The solid arrows in Figs. 10 and 11 marked “D1 and D2” indicate the increased indentation depth in the discrete track region at a load of 700  $\mu\text{N}$  compared to the indentation depth in the smooth surface area. Clearly, the load–displacement curves show that the contact deformation of discrete track media is affected by the aspect ratio of the groove and the land area.

Figure 12 shows the dissipated energy (Recco et al. 2009) as a function of normal load for the disks investigated in Figs. 9, 10, 11. The dissipated energy is the integral of the load displacement curve during a complete load-unload cycle. As can be seen from Fig. 12, the

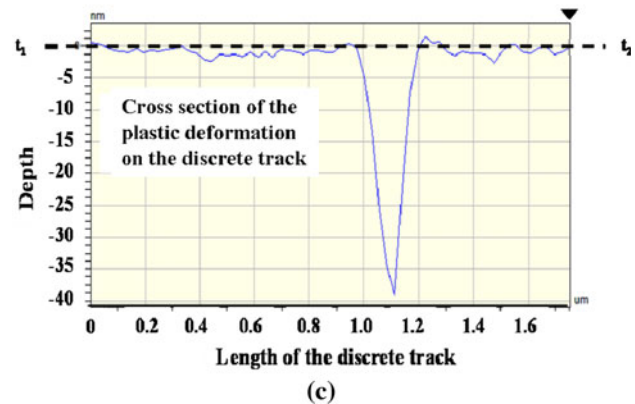
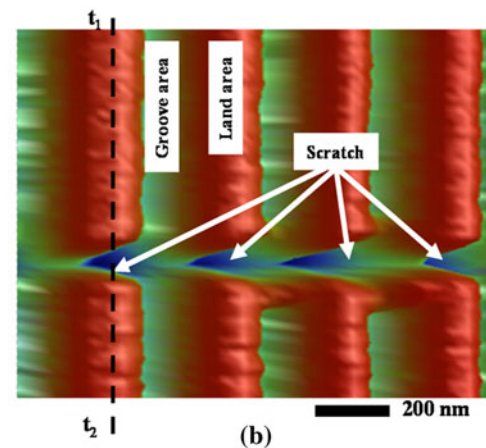
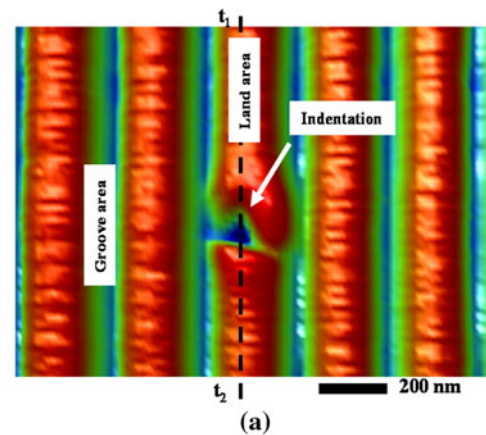


**Fig. 7** Indentation and scratch tests results on discrete track disks: **a** nano-indentation, **b** nano-scratch test and **c** typical cross section of plastic deformation of a discrete track along the line ( $t_1 - t_2$ )

dissipated energy for the smooth disk is smaller than the dissipated energy in the land area for either disk A or B. Furthermore, the dissipated energy for discrete track disk B, which has a smaller land width than disk A, is larger than the dissipated energy of disk A.

The residual indentation depth in the smooth and the land area of DTR disks A and B is shown in Fig. 13 as a function of the normal load. Clearly, the residual

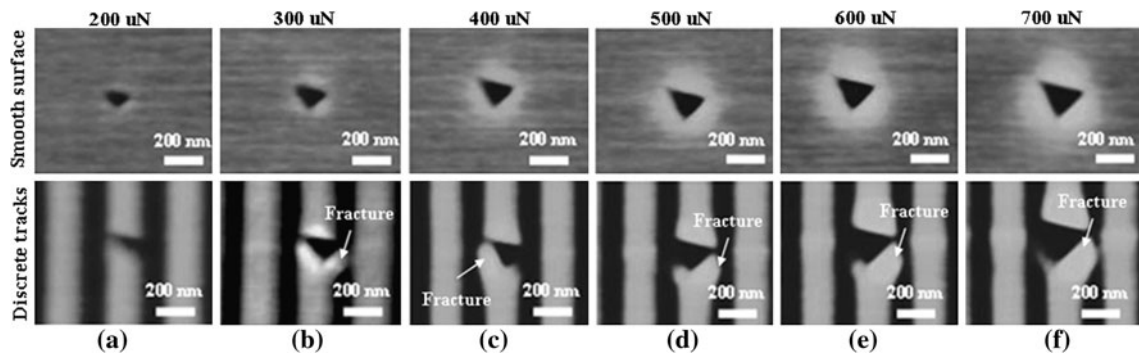


**Fig. 8** SPM images of nano-indentations on a smooth disk and the land area of a discrete track recording disk (discrete track disk B); a 200  $\mu\text{N}$ , b 300  $\mu\text{N}$ , c 400  $\mu\text{N}$ , d 500  $\mu\text{N}$ , e 600  $\mu\text{N}$  and f 700  $\mu\text{N}$

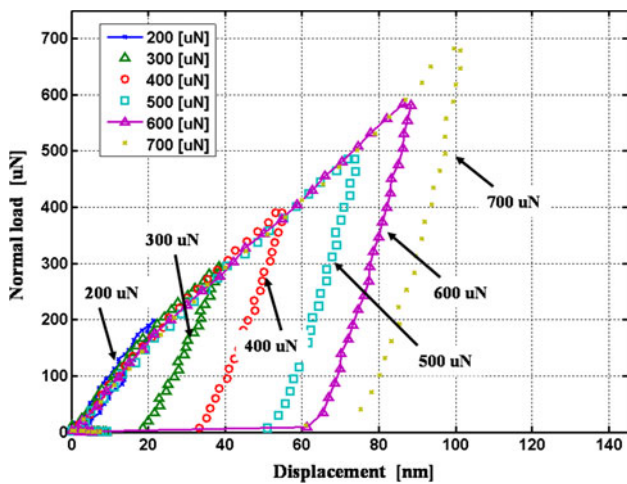


**Fig. 9** Load–displacement curves as a function of normal load in the smooth surface region

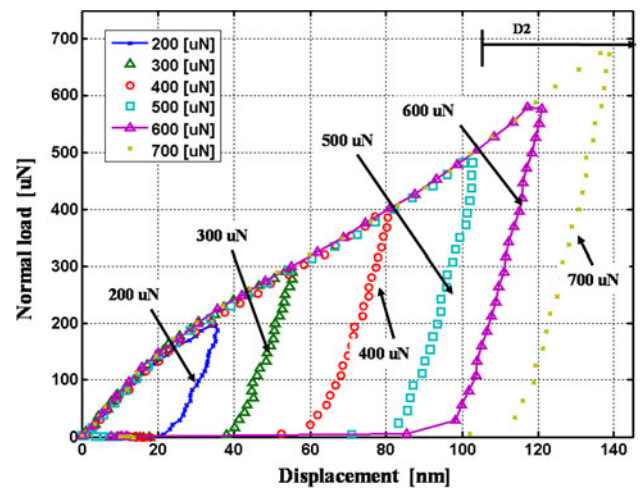


**Fig. 11** Load–displacement curves as a function of normal load in the land area of discrete track disk B

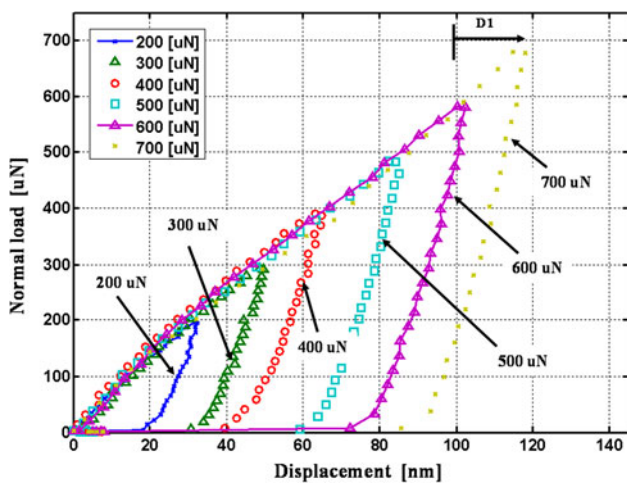


**Fig. 10** Load–displacement curves as a function of normal load in the land area of discrete track disk A

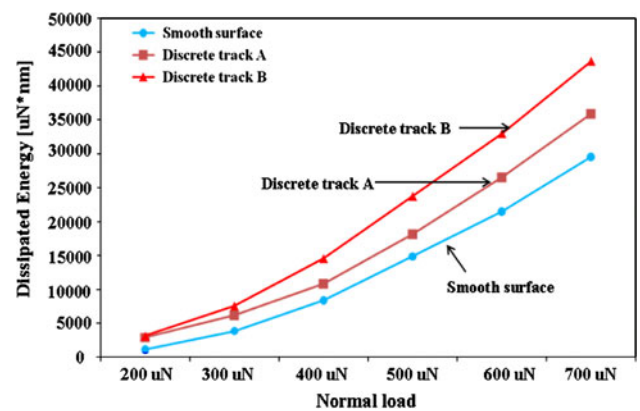


**Fig. 12** Dissipated energy versus normal load for different disk surfaces

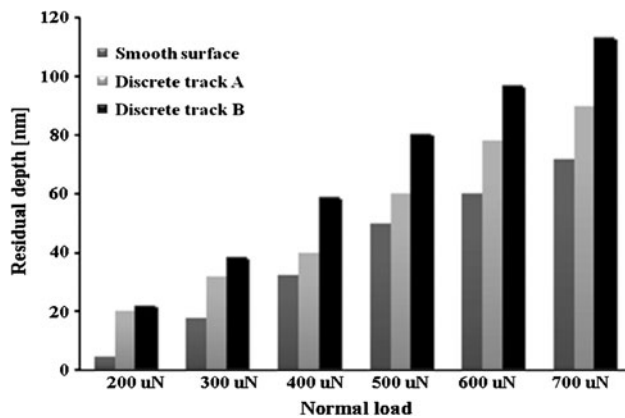


**Fig. 13** Residual indentation depth as a function of normal load

indentation depth increases with increasing normal load and is larger for the disk with narrower land width.

In the next series of experiments we performed nano-scratch tests (see Fig. 14) as a function of load using a lateral force microscope (Hysitron Inc.). A diamond cube corner tip was used at loads between 10 and 130  $\mu\text{N}$ . As can be seen from Fig. 14, the indentation depth was found to increase as a function of the normal load. Examining the photo micrographs, we also observe that the largest damage occurs at the edges of the discrete tracks. This result is in agreement with the numerical predictions from (Gong and Komvopoulos 2003).

Figure 15 shows the “wear” depth on smooth and discrete track disks A and B as a function of load during scratch testing. We observe that the wear depth of discrete track disks A and B is larger than that of the smooth surface, and that the wear depth of discrete track disk B, with the narrowest land width, is larger than that of discrete track disk A. This result is similar to the findings for the maximum residual indentation depth shown in Fig. 13.

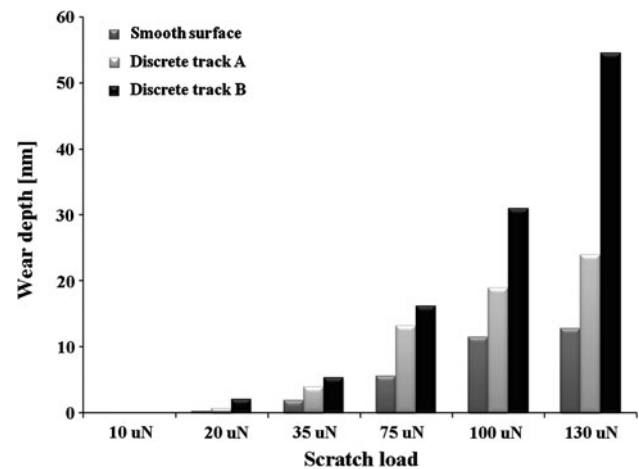


**Fig. 15** Wear depth as a function of scratch load on smooth disk area and discrete track disks A and B

### 3.3 Wear characteristics of discrete track media using reciprocating wear testing

Figure 16 shows SEM images of wear scars on smooth and discrete track disks at different loads and wear cycles using the reciprocating wear tester described in Sect. 2.3. We observe that the size of the wear scar increases with load and the number of cycles for smooth and discrete track disks. We also observe that the wear scars are smaller for a smooth disk (Fig. 16a–c) than for discrete track disks at the same experimental conditions (Fig. 16d–f). Furthermore, the number of wear particles generated in the discrete track area is substantially larger than the number of wear particles generated in the smooth area.

In Fig. 17, SEM images are shown for the spherical wear probe used in our reciprocating wear tests. We observe that a large amount of debris adheres to the wear

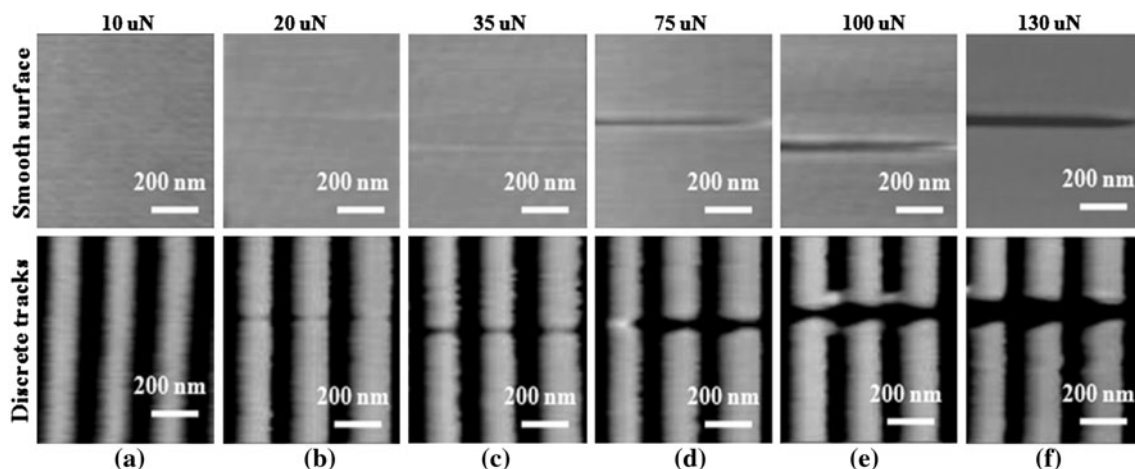


**Fig. 14** Typical SPM images of nano-scratch tests on smooth disk and discrete track disk B: **a** 10  $\mu\text{N}$ , **b** 20  $\mu\text{N}$ , **c** 35  $\mu\text{N}$ , **d** 75  $\mu\text{N}$ , **e** 100  $\mu\text{N}$  and **f** 130  $\mu\text{N}$

**Fig. 16** Comparison of wear scars on smooth and discrete track surfaces: **a** smooth disk area tested at 5 Hz/5.6  $\mu\text{m}$ /10  $\mu\text{N}$ /1,000, **b** smooth disk area tested at 5 Hz/5.6  $\mu\text{m}$ /20  $\mu\text{N}$ /1,000, **c** smooth disk area tested at 5 Hz/5.6  $\mu\text{m}$ /20  $\mu\text{N}$ /10,000, **d** discrete track surface tested at 5 Hz/5.6  $\mu\text{m}$ /10  $\mu\text{N}$ /1,000, **e** discrete track surface tested at 5 Hz/5.6  $\mu\text{m}$ /20  $\mu\text{N}$ /1,000 and **f** discrete track surface tested at 5 Hz/5.6  $\mu\text{m}$ /20  $\mu\text{N}$ /10,000

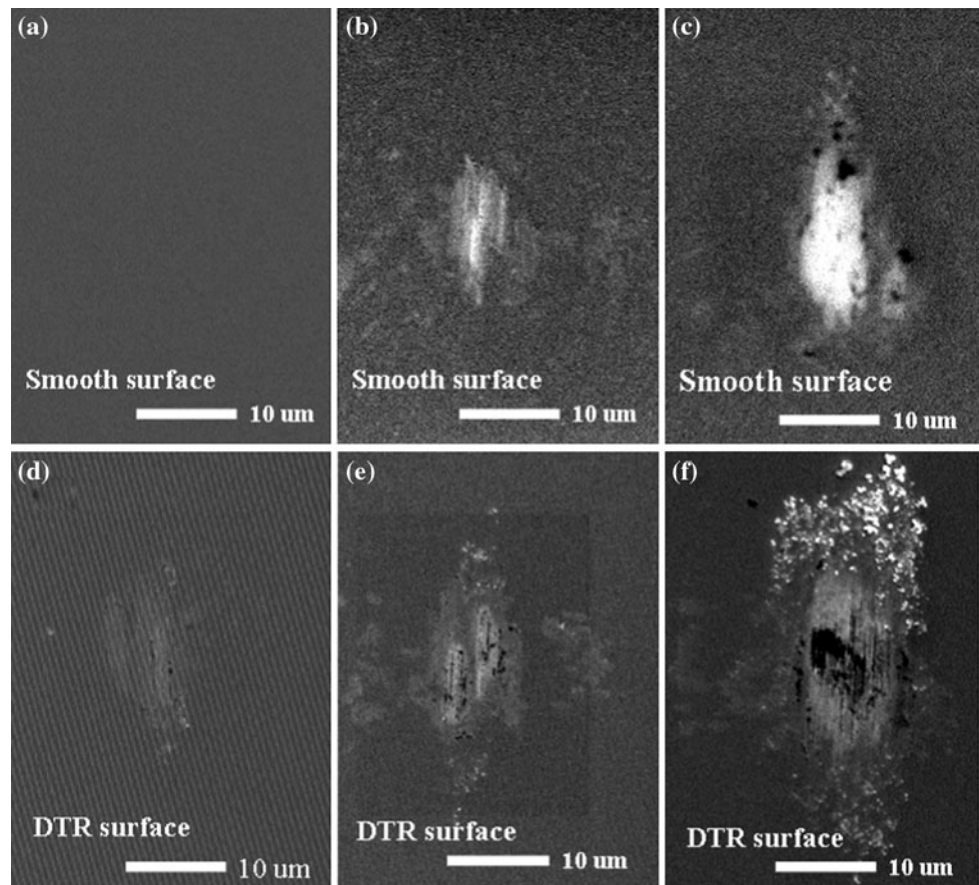
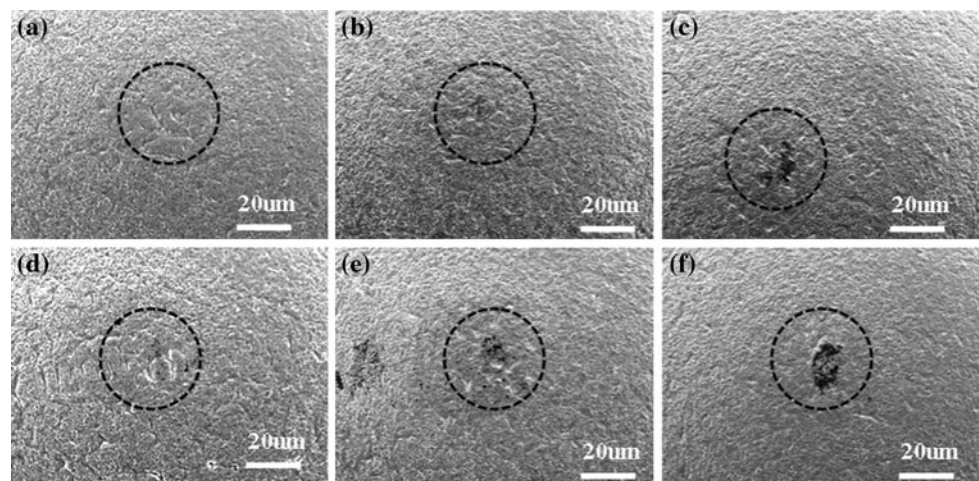


**Fig. 17** SEM images of spherical wear probe after reciprocating wear test: **a** with smooth disk at 5 Hz/5.6  $\mu\text{m}$ /10  $\mu\text{N}$ /1,000 cycles, **b** with smooth disk at 5 Hz/5.6  $\mu\text{m}$ /20  $\mu\text{N}$ /1,000 cycles, **c** with smooth disk at 5 Hz/5.6  $\mu\text{m}$ /20  $\mu\text{N}$ /10,000 cycles, **d** with discrete track surface at 5 Hz/5.6  $\mu\text{m}$ /10  $\mu\text{N}$ /1,000 cycles, **e** with discrete track surface at 5 Hz/5.6  $\mu\text{m}$ /20  $\mu\text{N}$ /1,000 cycles and **f** with discrete track surface at 5 Hz/5.6  $\mu\text{m}$ /20  $\mu\text{N}$ /10,000 cycles

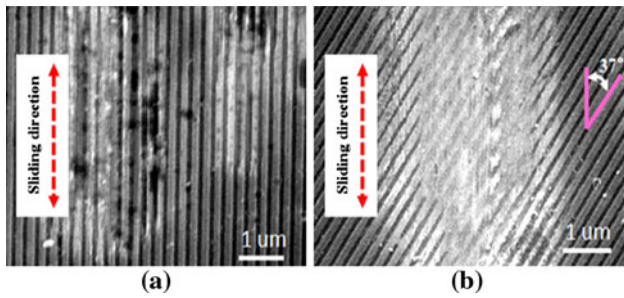


probe and that the amount of adhering wear particles is greater for DTR disks than for smooth disks.

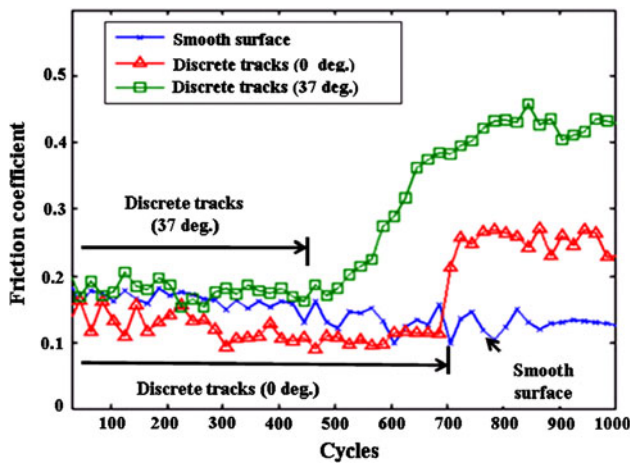
Figure 18a, b show SEM images of discrete track disks after reciprocating wear testing at an angle of  $37^\circ$  to the track directions. We observe that the damage of the discrete track area is more severe at an oblique angle than at  $0^\circ$ , i.e., discrete tracks are damaged more easily during reciprocal sliding if the direction of sliding is not parallel to the track direction.

Figure 19 shows the variation of the coefficient of friction as a function of wear cycles. We observe that the friction coefficient increases with the number of cycles for the discrete track surface, while the coefficient of friction remains constant on the smooth surface. The increase in the friction coefficient is found to occur earlier for the oblique sliding case than for the zero angle case.

Figure 20a shows the Raman spectrum of a DLC coated disk before wear testing. Figure 20b, c show Raman



**Fig. 18** SEM images of wear scars of discrete track region for different sliding directions: **a** 0° and **b** 37°



**Fig. 19** Friction coefficients as a function of cycles on smooth surface and discrete track disk at 5 Hz/5.6 μm/10 mN/1,000 cycles

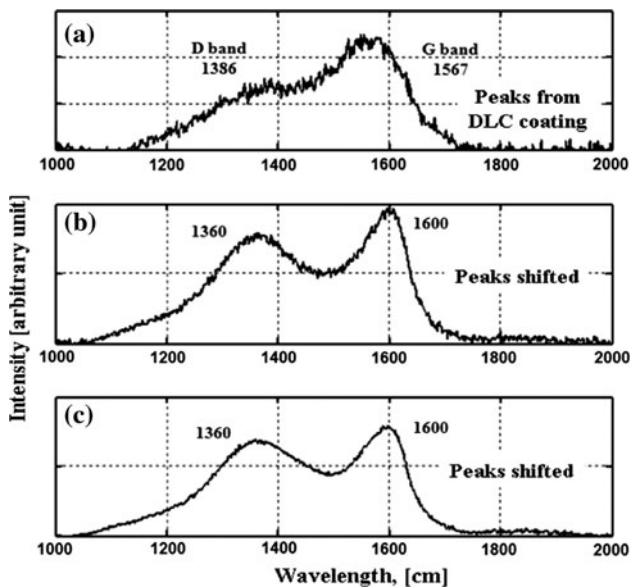


**Fig. 20** Raman spectra of **a** DLC film before reciprocating wear testing **b** wear particles from the discrete track surface and **c** wear particles from the smooth disk area

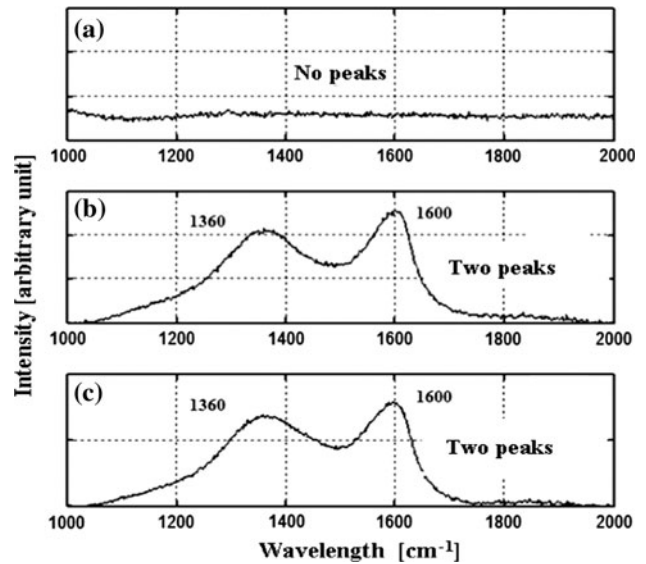


**Fig. 21** Raman spectra on spherical wear probe **a** before wear testing, **b** after wear testing on discrete track disk and **c** after wear testing on smooth disk

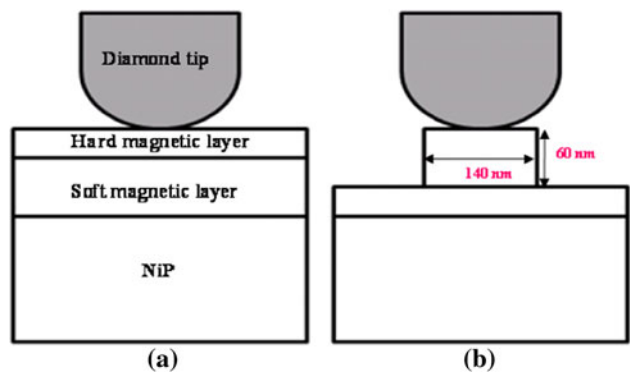


**Fig. 22** Schematic of contact model for **a** smooth surface and **b** discrete track disk (groove depth = 60 nm and land width = 140 nm)

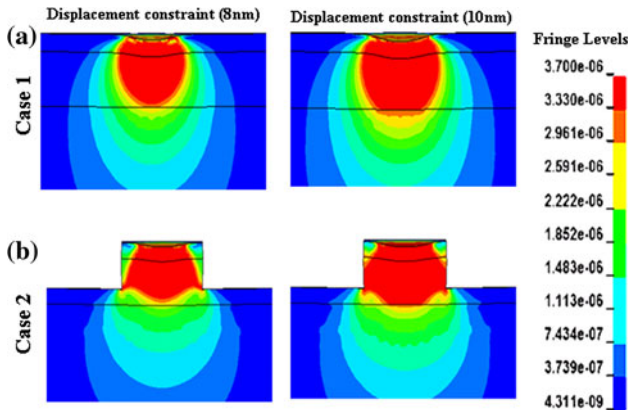
spectra of wear particles found on the discrete track disk and the smooth disk, respectively. The Raman spectrum in Fig. 20a shows peaks at 1,567 and 1,386 per cm, commonly referred to as G band (sp<sup>2</sup>) and D band (sp<sup>3</sup>) (Irmer and Dorner-Reisel 2005). A slight shift of the peaks is observed in Figs. 20b, c (1,600 and 1,360 per cm) for the Raman spectra of the wear particles.

Figure 21a, b, c show Raman spectra of the spherical wear probe. We observe that no peaks are present (Fig. 21a) for the spherical wear probe before reciprocating wear testing. However, the Raman spectra after wear testing show two distinct peaks at a reciprocal wavelength of 1,360 and 1,600 per cm, respectively (Fig. 21b, c). Clearly, this change in the Raman spectrum is due to the presence of adhering wear particles on the wear probe from the disks after reciprocating wear testing.



**Table 2** Material properties of diamond tip and different layers of discrete track disk (Ovcharenko et al. 2010)

	Tip	Hard magnetic layer (20 nm)	Soft magnetic layer (60 nm)	NiP (200 nm)
<i>E</i> (GPa)	1,140	150	120	114
Poisson’s ratio	0.07	0.3	0.3	0.31
Yield stress (GPa)	35.7	3.4	3.7	3.0



**Fig. 23** Von Mises stress contour on **a** smooth disk and **b** discrete track disk (groove depth = 60 nm and land width = 140 nm) (stress is measured in  $10^6$  GPa)

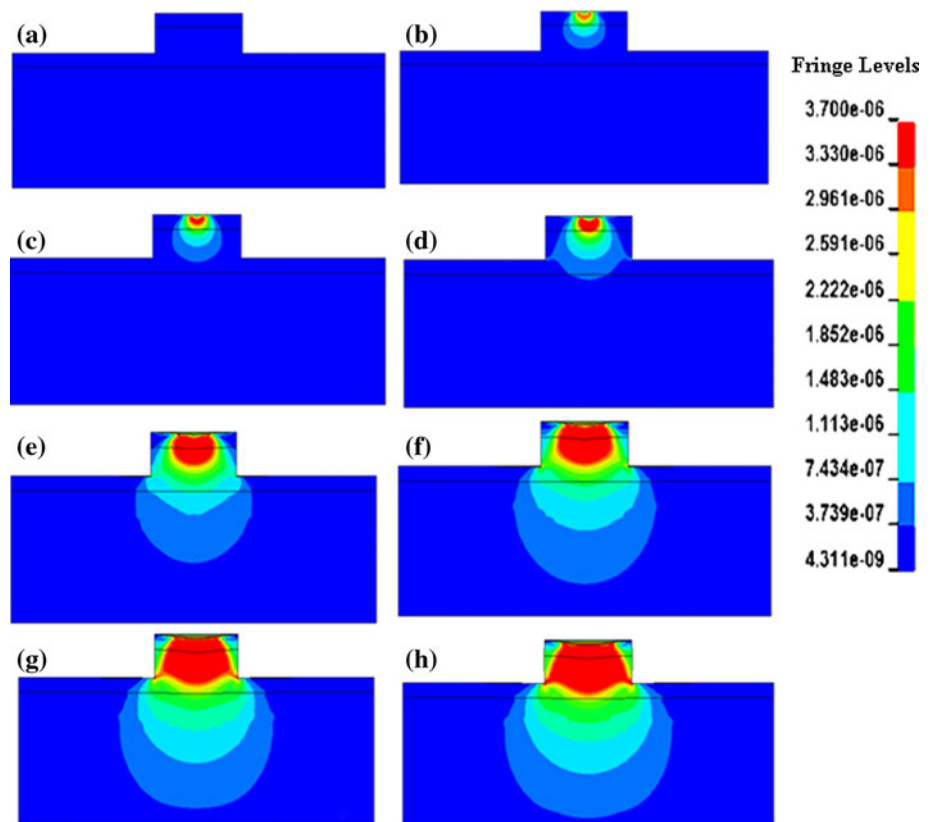
#### 4 Numerical investigation of static contact behavior

To correlate our experimental results with numerical predictions, a finite element analysis was performed for the static contact deformation using the commercially available software LS-DYNA.

Figure 22a shows the contact model for a smooth disk surface, while Fig. 22b shows the contact model for a discrete track surface.

Table 2 shows the material properties used for the finite element investigation. The thicknesses of the hard magnetic layer, the soft magnetic layer and the NiP layer were assumed to be 20, 60 and 200 nm, respectively. Figure 23 shows von Mises stress contours for a smooth disk (case 1) and a discrete track disk (case 2). We observe high stress concentrations at the corners of the discrete tracks,

**Fig. 24** Von Mises stress distribution on discrete track (stress is measured in  $10^6$  GPa)



indicating that yielding of the discrete track is likely to occur at those locations. Clearly, high stress concentrations at the corners of discrete tracks can initiate cracks or damage of the discrete tracks (see Fig. 8).

Figure 24 shows the evolution of the von Mises stress in a discrete track disk as a function of indentation load. Figure 24a shows the un-deformed case prior to contact. In the initial phase of contact (Fig. 24b through c), the stress distribution is similar to the case of a smooth surface (see Figs. 23a). However, as the contact load is increased, the yield stress contour increases reaching the corner at the bottom of the discrete track (see Fig. 24d through Fig. 24h). Clearly, this situation is critical with respect to wear and initiation of failure.

## 5 Summary and conclusions

An experimental investigation of contact deformation and wear characteristics of discrete track and smooth disk surfaces was performed. Damage was found to be much larger in the land areas of discrete track disks than the smooth areas of the same disks. It is apparent that the stresses in the land areas of a discrete track disk are higher than the stresses in the smooth region of a disk under identical loads. The land area showed substantially higher wear and damage than the smooth areas outside the discrete track region. The latter results are a consequence of the presence of the unsupported edges of the narrow land areas of individual discrete tracks. From the data obtained we conclude that wear and damage increase with decreasing land width of discrete track disks. Numerical calculations are in agreement with experimental observations.

The generation of wear particles in discrete track disks increases the possibility of failure of hard disk drives during contacts between slider and disk. Therefore, to improve reliability and durability of DTR media, contact deformation and wear characteristics of discrete track media must be improved. Planarization of discrete track disks appears to be a necessary step towards improving the tribological properties of discrete track disks.

**Open Access** This article is distributed under the terms of the Creative Commons Attribution Noncommercial License which permits any noncommercial use, distribution, and reproduction in any medium, provided the original author(s) and source are credited.

## References

- Anoikin EV, Yang MM, Chao JL, Elings JR, Brown DW (1998) Nanoscale scratch resistance of ultrathin protective overcoats on hard magnetic disks. *J Vac Sci Technol A* 16:1741–1744
- Bai M, Kato K, Umehara N, Miyake Y, Xu J, Tokisue H (2000) Scratch-wear resistance of nanoscale super thin carbon nitride overcoat evaluated by AFM with a diamond tip. *Surf Coat Technol* 126:181–194
- Bhushan B (1999) *Handbook of micro/nano Tribology*, 2nd edn. CRC press LLC, UK, pp 433–524
- Bhushan B (2001) Nano-to microscale wear and mechanical characterization using scanning probe microscopy. *Wear* 251:1105–1123
- Gong Z-Q, Komvopoulos K (2003) Effect of surface patterning on contact deformation of elastic-plastic layered media. *Trans ASME* 125:16–24
- Greaves SJ, Muraoka H (2006) Discrete track media for 600 Gbits/in<sup>2</sup> recording. *J Appl Phys* 99:08F903
- Huang L-Y, Xu K-W, Lu J, Guelorget B, Chen H (2001) Nanoscratch and fretting wear study of DLC coatings for biomedical application. *Diam Relat Mater* 10:1448–1456
- Irmer G, Dörner-Reisel A (2005) Micro-Raman studies on DLC coatings. *Adv Eng Mater* 7(8):694–705
- Jiang Z, Lu C-J, Bogy DB, Bhatia CS, Miyamoto T (1995) Nanotribological characterization of hydrogenated carbon films by scanning probe microscopy. *Thin Solid Films* 258:75–81
- Juang J-Y, Bogy DB, Bhatia CS (2007) Design and dynamics of flying height control slider with piezoelectric nanoactuator in hard disk drives. *J Tribol* 129:161–170
- Kohira H, Tanaka H, Matsumoto M, Talke FE (2001) Investigation of slider vibrations due to contact with a smooth disk surface. *Trans ASME* 123:616–623
- Komvopoulos K (2000) Head-disk interface contact mechanics for ultrahigh density magnetic recording. *Wear* 238:1–11
- Li X, Bhushan B (1999) Micro/nanomechanical and tribological characterization of ultrathin amorphous carbon coatings. *J Mater Res* 14(6):2328–2337
- Nunez EE, Yeo C-D, Katta RR, Polycarpou A (2008) Effect of planarization on the contact behavior of patterned media. *IEEE Trans Magn* 44(11):3667–3670
- Ovcharenko A, Yang M, Chun K, Talke FE (2010) Simulation of magnetic erasure due to transient slider-disk contacts. *IEEE Trans Magn* 46:770–777
- Recco AAC, Viafara CC, Sinatora A, Tschiptschin AP (2009) Energy dissipation in depth-sensing indentation as a characteristic of the nanoscratch behavior of coatings. *Wear* 267:1146–1152
- Sundararajan S, Bhushan B (1999) Micro/nanotribology of ultra-thin hard amorphous carbon coatings using atomic force/friction force microscopy. *Wear* 225–229:678–689
- Wachenschwanz D, Jiang W, Roddick E, Homola A, Dorsey P, Harper B, Treves D, Bajorek C (2005) Design of a manufacturable discrete track recording medium. *IEEE Trans Magn* 41(2):670–675
- Wang R-H, Nayak V, Huang F-Y, Tang W, Lee F (2001) Head-disk dynamics in the flying, near contact, and contact regimes. *J Tribol* 123:561–565
- Weller D, Moser A (1999) Thermal effect limits in ultrahigh-density magnetic recording. *IEEE Trans Magn* 35:4423–4439
- Xu J, Tokisue H, Tanaka H, Matsumoto M (2002) Contact vibration of micro-textured sliders. *J Tribol* 124:281–287